Supporting Information

First-principles investigation on improved electron/ion transport and oxygen stability of Mo-doped Li_2MnO_3

Yurui Gao,[a] Jun Ma,[a] Xuefeng Wang,[a] Xia Lu,[a] Ying Bai,[b] Zhaoxiang Wang,*[a] and Liquan Chen[a]

[a]*Key Laboratory for Renewable Energy, Beijing Key Laboratory for New Energy Materials and Devices, Beijing National Laboratory for Condensed Matter Physics, Institute of Physics, Chinese Academy of Sciences, P. O. Box 603, Beijing 100190, China. *Email: zxwang@iphy.ac.cn Tel: +86-10-82649050 Fax: +86-10-82649050.*

[b]*Key Laboratory of Photovoltaic Materials of Henan Province and School of Physics and Electronics, Henan University, Kaifeng 475004, China*

Materials Preparation and Characterization

Li_2MnO_3 and Mo-doped $Li_2Mn_{1-x}Mo_xO_3$ (x = 0.05, 0.10, 0.15, 0.20) powders were synthesized by solid-state reaction with Li_2CO_3, $MnCO_3$ and MoO_3 as precursors at appropriate atomic ratios. To compensate for the possible Li loss during high temperature annealing, excess of

Li_2CO_3 (5 mol%) was added. The precursors were mixed by milling in absolute ethyl ethanol and then annealed at 800 °C for 24 h in air. The structure of the obtained powders was characterized on an X'Pert Pro MPD X-ray diffractometer (XRD, Philips, Holland) with monochromatized Cu Kα radiation (λ = 1.5405 Å).

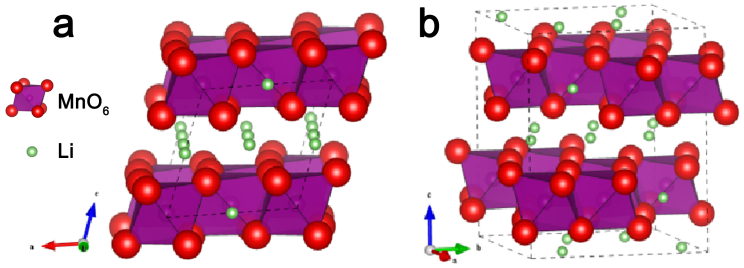

Fig. S1 The primitive cell of Li_2MnO_3: (a) C2/m; (b) C2/c.

As the symmetry of C2/m is higher than that of C2/c, the primitive cell of *m*-Li_2MnO_3 is nearly half that of *c*-Li_2MnO_3.

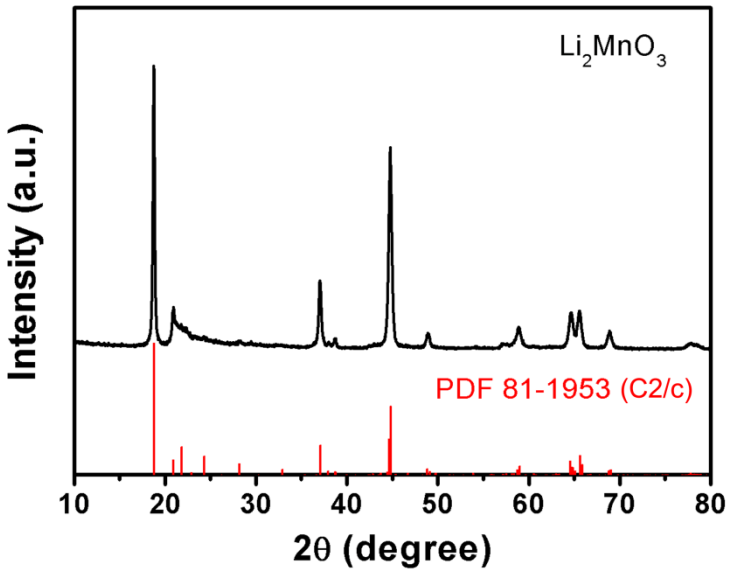

Fig. S2 XRD of the Li_2MnO_3 prepared by the solid-state reaction.

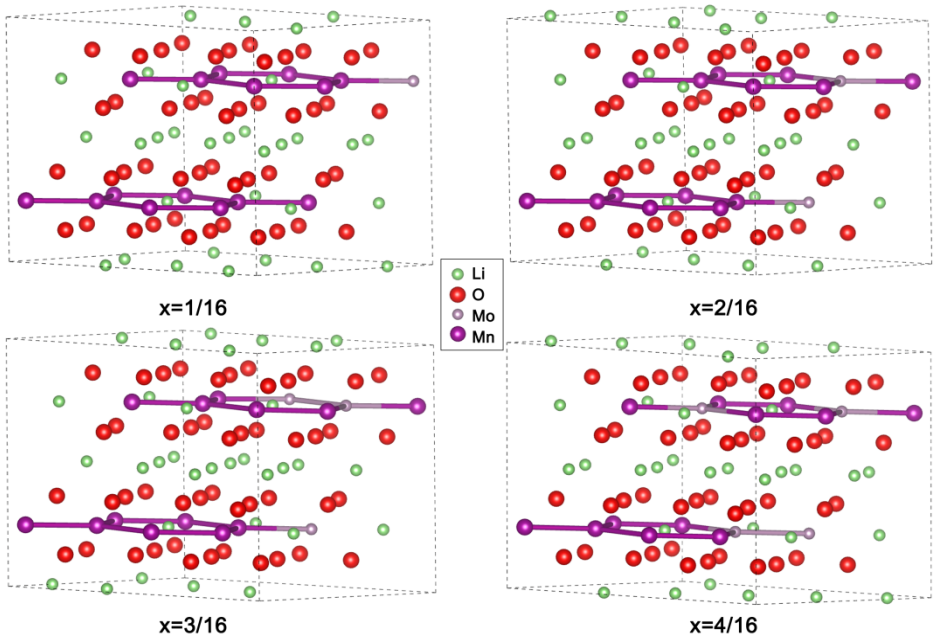

Fig. S3 Ground state of $Li_2Mn_{1-x}Mo_xO_3$ (x =1/16, 2/16, 3/16 and 4/16).

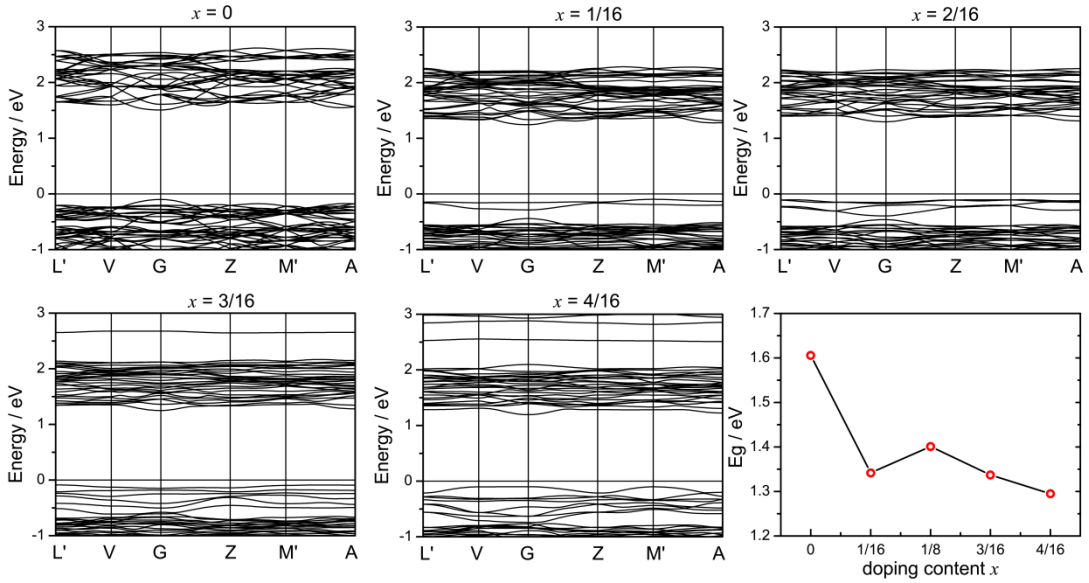

Fig. S4 Band structures (spin up) of $Li_2Mn_{1-x}Mo_xO_3$ (x =1/16, 2/16, 3/16 and 4/16) and the width of the forbidden gap against x.

Fig. S4 shows the band structure (spin up) of $Li_2Mn_{1-x}Mo_xO_3$ and the width of forbidden gap

against x. Electron bands appear in the forbidden gap and the width of the forbidden gap decreases when Mo is doped. In addition, the number of the doping electron bands increases gradually as x increases from 1/16 to 4/16, in agreement with the results of the DOS analysis (Fig. 2c). As a result, the conductivity is expected to be increased with Mo doping. This is supported with the color change of the home-prepared Mo-doped Li_2MnO_3.

As *m*-Li_2MnO_3 and *c*-Li_2MnO_3 show similar electronic structures while the home-prepared Li_2MnO_3 shows a C2/c phase (Fig. S2), *c*-Li_2MnO_3 is adopted as the mother body in the following Mo doping investigation.

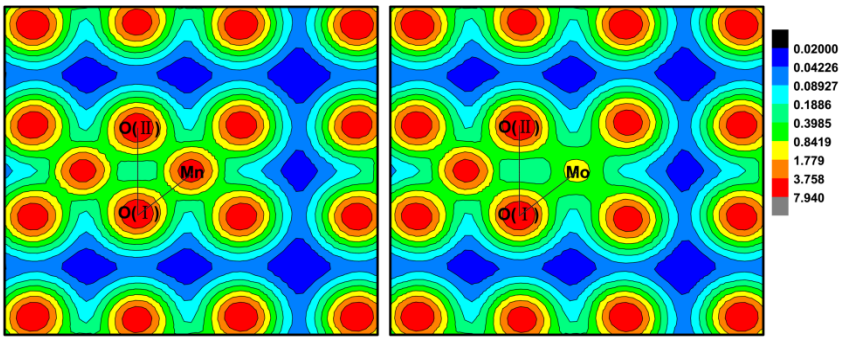

Fig. S5 Charge density on a plane through (a) one Mn atom, its nearest-neighbor O(Ⅰ) and O(Ⅱ) in Li_2MnO_3; (b) the Mo atom, its nearest-neighbor O(Ⅰ) and O(Ⅱ) in $Li_2Mn_{1-x}Mo_xO_3$ (x = 1/16).

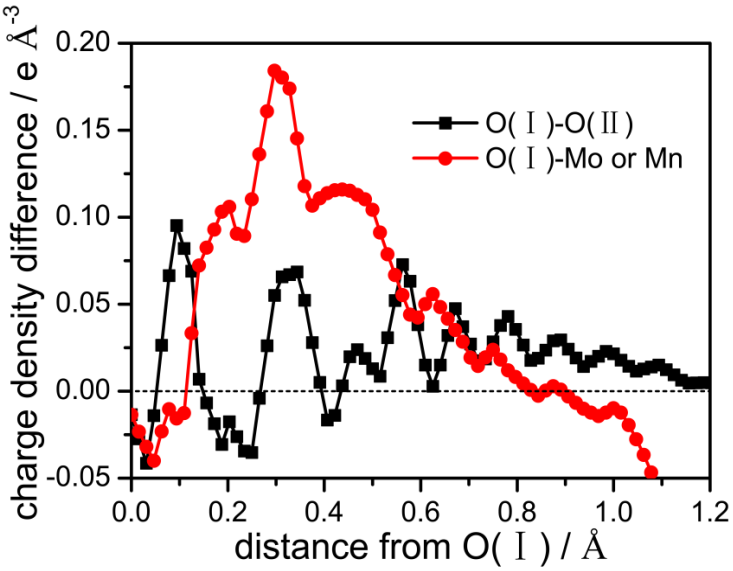

Fig. S6 The extra charge density, $\rho_{[Li2Mn1-xMoxO3]} - \rho_{[Li2MnO3]}$ (x = 1/16) along the line O(I)-O(II) and line O(I)-M (M=Mo, Mn), vs. the distance from O(I).

Fig. S5 shows the charge density on a plane through one Mn or Mo atom, its nearest neighbor O(I) and O(II) in Li_2MnO_3 and $Li_2Mn_{1-x}Mo_xO_3$ (x = 1/16), respectively. The charge density difference between Li_2MnO_3 and $Li_2Mn_{1-x}Mo_xO_3$ along the O(I)–O(II) and the O(I)–M (M = Mo, Mn) lines is shown in Fig. S6. Clearly there is more positive charge than negative charge along both lines, consistent with the Bader charge analysis.

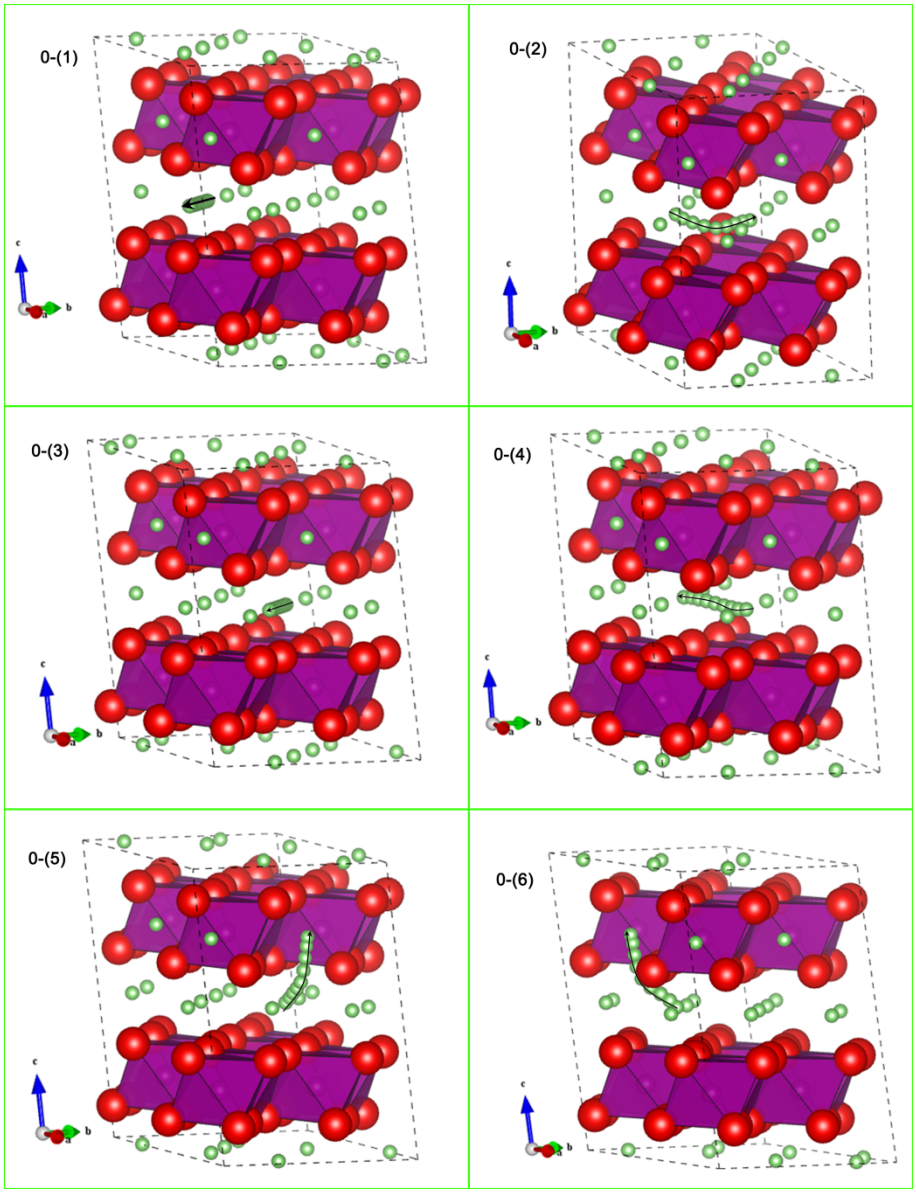

Fig. S7 Diffusion pathways of $Li_2Mn_{1-x}Mo_xO_3$ at x=0 (Li_2MnO_3).

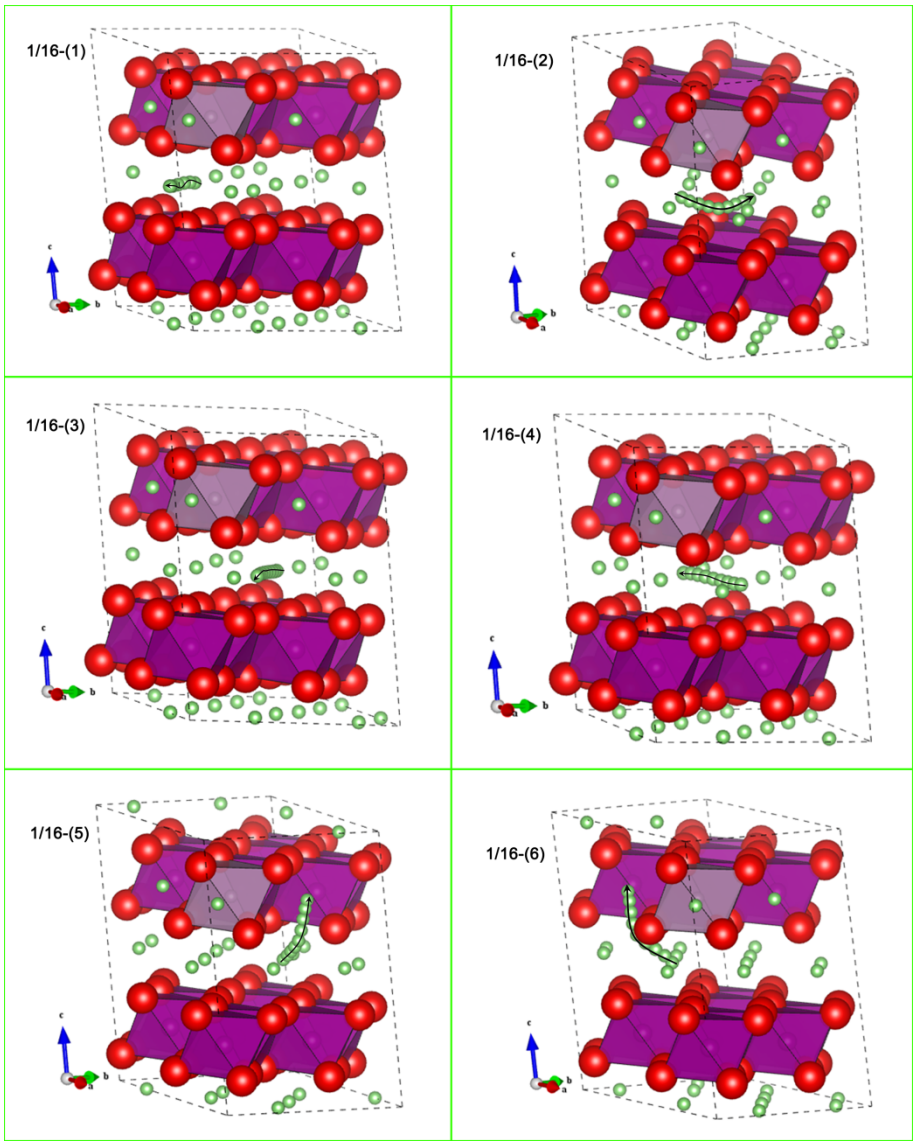

Fig. S8 Diffusion pathways of $Li_2Mn_{1-x}Mo_xO_3$ at x=1/16.

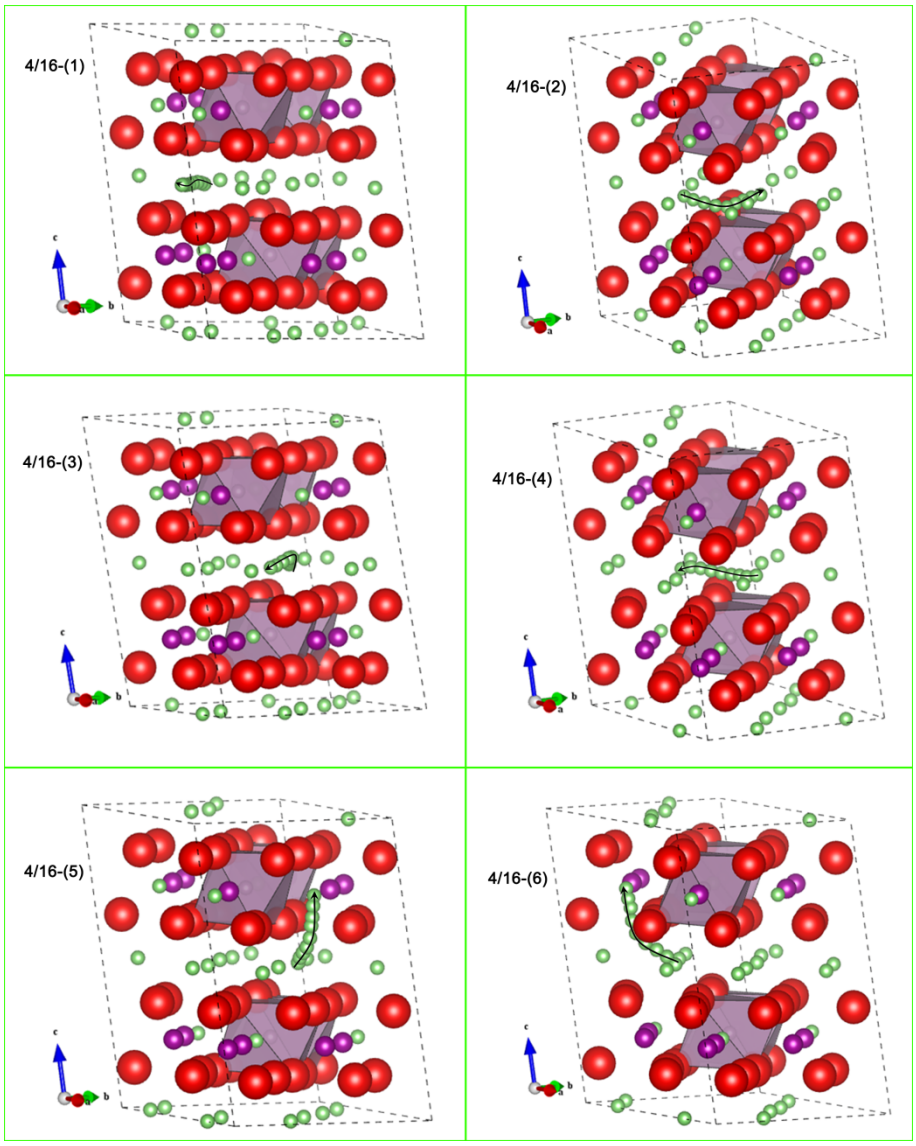

Fig. S9 Diffusion pathways of $Li_2Mn_{1-x}Mo_xO_3$ at x=4/16.

Electrical conductivity measurement

The electrical conductivity measurements for Li_2MnO_3 and Mo-doped Li_2MnO_3 ceramic disks were performed by the AC impedance spectroscopy using an impedance/gain-phase analyzer (SI 1260, Solartron Metrology) between 100 Hz and 1 MHz. For ceramic disks preparation, the Li_2MnO_3 and Mo-doped Li_2MnO_3 precursors were firstly synthesized using appropriate ratio of Li_2CO_3, $MnCO_3$ and MoO_3 by a solid state reaction at 550 °C for 4 h in air. Then, the obtained precursors were grinded and separately mixed with a small amount of polyvinyl alcohol (PVA) as binder and pressed into a disk shaped pellet with about 15 mm diameter and 1-2 mm thickness

under a mono-axial pressure of 14 MPa. The ceramic disks were sintered at 800 ºC for 24 h in air. Silver electrodes were printed on both surfaces and subsequently fired at 500 ºC for 15 min before electrical conductivity measurements.

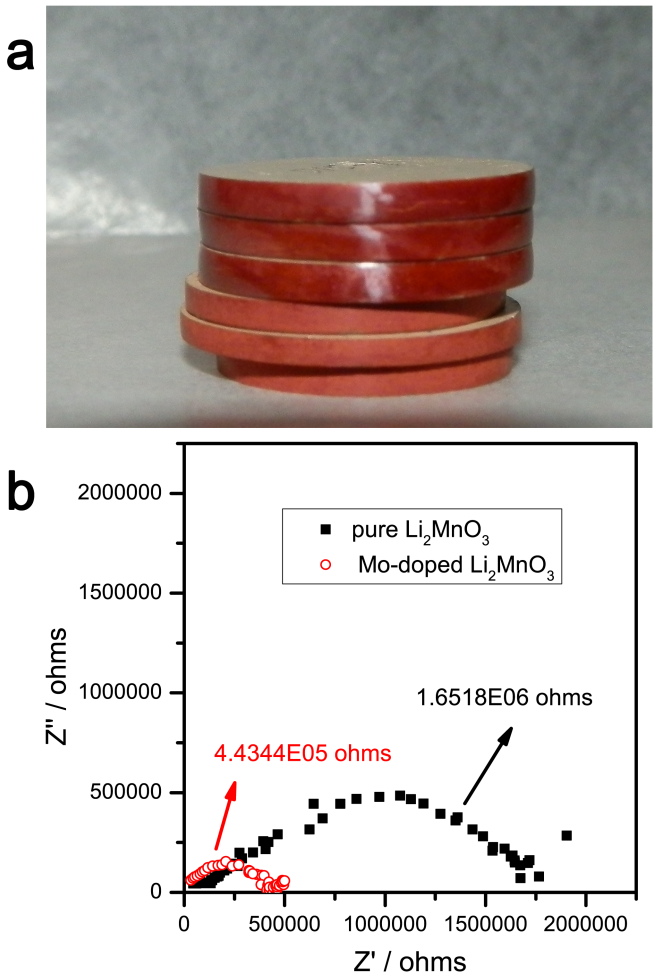

Fig. S10 (a) The ceramic disks of the pristine and 15% Mo-doped Li_2MnO_3. The above three are ceramic disks of the pristine Li_2MnO_3 and the bottom three are ceramic disks of $Li_2Mn_{0.85}Mo_{0.15}O_3$. (b) AC impedance spectroscopy for the pristine and $Li_2Mn_{0.85}Mo_{0.15}O_3$ at room temperature.

According to the equations

$$\rho_T = \frac{R_T s}{h}$$

$$\sigma_T = \frac{1}{\rho_T}$$

the electrical conductivity σ can be obtained as follows:

for the pristine Li_2MnO_3,

h_1=0.1204 cm

S_1=1.268520 cm^2

ρ_1 =1.74032E7 Ω·cm

σ_1 = 5.74607E-6 S/m

for $Li_2Mn_{0.85}Mo_{0.15}O_3$,

h_2= 0.1424 cm

S_2=1.577528 cm^2

ρ_2 =4.91249E6 Ω·cm

σ_2 =2.03563E-5 S/m

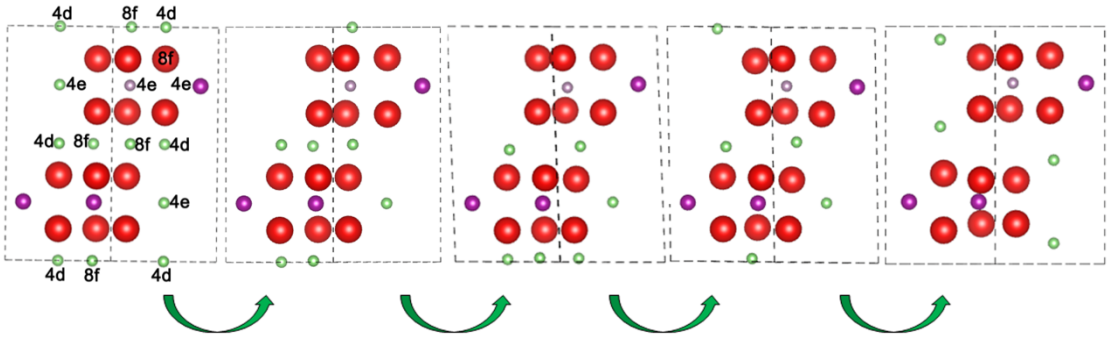

Fig. S11 Simulation of Li removal $Li_2Mn_{0.75}Mo_{0.25}O_3$ (the ground state structures of $Li_yMn_{0.75}Mo_{0.25}O_3$ with y=2, 1.75, 1.5, 1.25 and 1).

Table S1. Calculated volume change of $Li_2Mn_{1-x}Mo_xO_3$ (x = 1/16, 2/16, 3/16, 4/16) by PBE+U

(U_{eff}=4.9, 6.3 eV for Mn and Mo respectively, or U_{eff}=4.9 eV for Mn while Mo without U calibration) method.

Mo content *x*	Volume ($Å^3$ $f.u.^{-1}$)	Volume expansion (%)	Volume* ($Å^3$ $f.u.^{-1}$)	Volume expansion* (%)
0	51.873	---	51.873	---
1/16	52.795	1.777	53.043	2.255
2/16	53.356	2.859	53.926	3.958
3/16	53.899	3.906	54.930	5.893
4/16	54.523	5.109	56.005	7.966

Notes: * result of Mo without U calibration.